

Supplementary materials for

Far-field Super-resolution Imaging By Nonlinearly Excited Evanescent Waves

Zhihao Zhou¹, Wei Liu², Jiajing He¹, Lei Chen², Xin Luo¹, Dongyi Shen²,
Jianjun Cao³, Yaping Dan¹, Xianfeng Chen² and Wenjie Wan^{1,2*}

¹The State Key Laboratory of Advanced Optical Communication Systems and Networks,
University of Michigan-Shanghai Jiao Tong University Joint Institute,
Shanghai Jiao Tong University, Shanghai 200240, China

²MOE Key Laboratory for Laser Plasmas and Collaborative Innovation Center of IFSA,
School of Physics and Astronomy, Shanghai Jiao Tong University, Shanghai 200240, China

³School of Science, Jiangnan University, Wuxi 214122, China

* Corresponding author: Wenjie Wan wenjie.wan@sjtu.edu.cn

S1. Four-Wave Mixing's (FWM) prerequisite: Optical Parametric Oscillator (OPO)

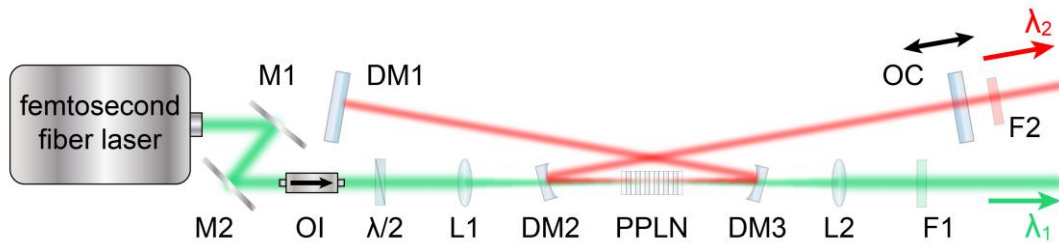


Fig. S1 Setup of our customized OPO

The setup of our OPO is shown in Fig. S1. (M: mirror, L: lens, OI: optical isolator, $\lambda/2$: half-wave plate, DM: dielectric mirror, PPLN: periodic-poled lithium niobate, F: color filter, OC: output coupler.) We use the frequency-doubled output of a fiber femtosecond laser (Fianium FemtoPower 1064/532-fs) delivering pulses at 532nm, with time duration ~ 200 fs and 80MHz repetition rate, as the pump beam. A singly-resonant, bow-tie cavity is built up for the signal beam to oscillate around. The length of the cavity is carefully tuned to make the signal pulse meet the next pump pulse after traveling for a round trip. When they meet up together inside the nonlinear PPLN crystal, the signal pulse will experience parametric amplification. By repeating the process over and over in the cavity, significant output signal will be generated at the output coupler (OC). The excited signal's pulse-width has a similar duration with the pump beam.

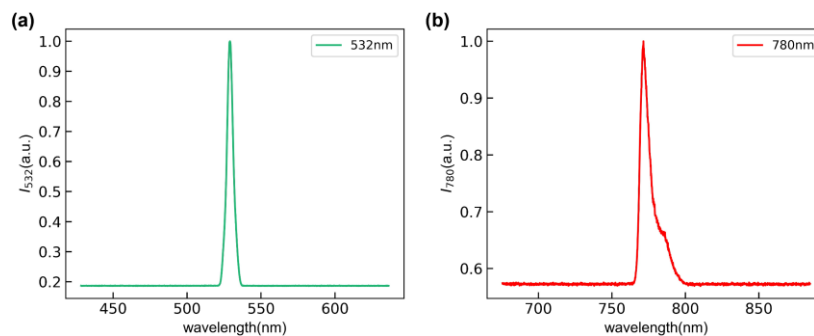


Fig. S2 Wavelength spectrum of (a) pump and (b) signal beams

Wavelength spectrums of these two beams are shown in Fig. S2. The signal's wavelength can be tuned either by changing temperature of MgO:PPLN crystal (Covesion Ltd.) or utilizing different periods of PPLN, making the OPO's output cover a wide spectral range. The residual part of the pump beam, which is transmitted through DM3, is collected and shaped by lens L2. It will be used in four-wave mixing (FWM) experiment later as the pump beam. (Note that we call λ_2 as signal beam here, but later in FWM experiment we call it probe beam instead.)

S2. Nonlinear Four-Wave Mixing (FWM) and Efficiency for Evanescent Generation

The third-order nonlinear response of the medium acts as the source term of four-wave mixing signal at $2\omega_1 - \omega_2$, which reads:

$$\mathbf{P} = \varepsilon_0 \chi_{ijkl}^{(3)}(\omega_{FWM} = \omega_1 + \omega_1 - \omega_2) \mathbf{E}_1 \mathbf{E}_1 \mathbf{E}_2^*$$

where \mathbf{E}_i are the incident electric field vectors and $\chi_{ijkl}^{(3)}$ is third-order susceptibility of the nonlinear medium. The wavelength spectrum of excited FWM signal is shown in Fig. S3.

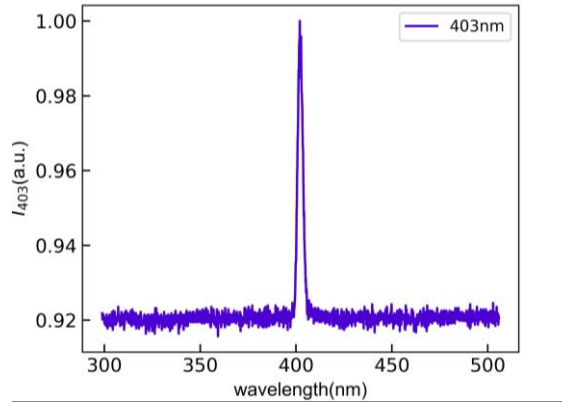


Fig. S3 FWM signal spectrum excited by FWM process $2\omega_1 - \omega_2$

From the above relation, the FWM signal's power should depend quadratically on the input pump beam power $P(\omega_1)$ and linearly on $P(\omega_2)$. The signal power's dependences on pump/probe beams are measured experimentally and shown in Fig. S4, in which both the horizontal and vertical axes are logarithmically scaled. Of which the linear fitted slopes are 1.91 and 1.03, respectively. Besides, the signal's intensity versus time delay between pump and probe beams are measured as a result of cross-correlation between the two pulses [Fig. S5]. The measured time duration is about 240fs.

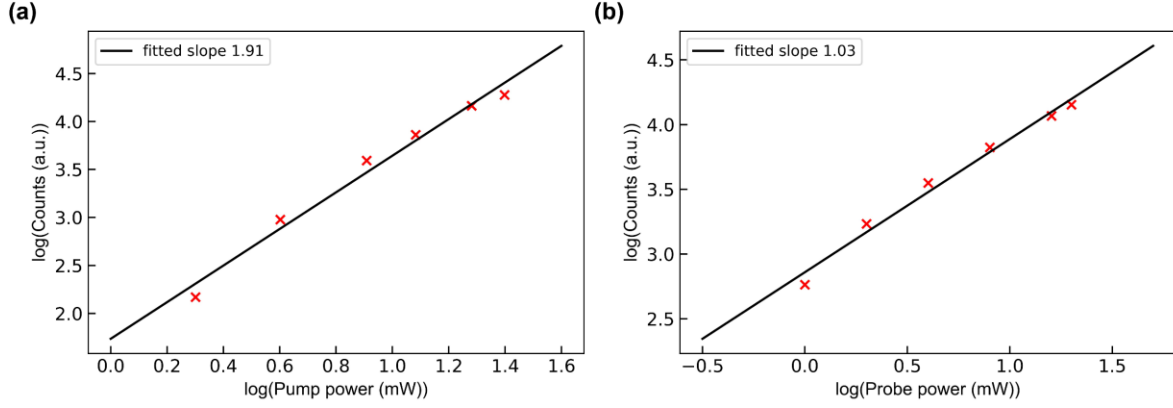


Fig. S4 FWM signal's power dependences on (a) pump and (b) probe beams

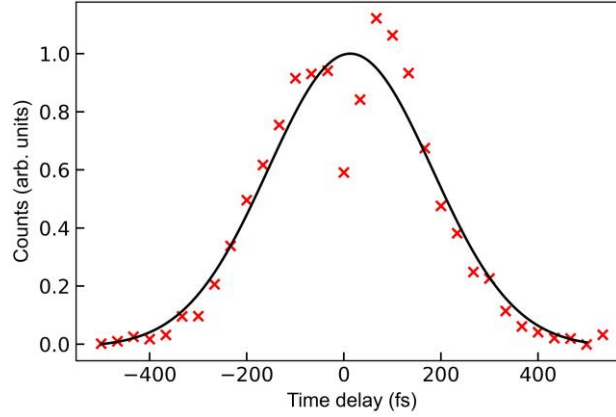


Fig. S5 FWM signal as a function of pump/probe beams' relative time delay

In our experiment, the pump/probe beams are on the level of 10mW and 4mW, respectively, corresponding to peak intensities of $5GW/cm^2$ and $2GW/cm^2$ (the diameter of spot area is $\sim 4\mu m$). After calibrating the power of evanescent FWM signal by correction of quantum efficiency (QE) of EMCCD and comparing signal counts with known power of pump beam, we get the efficiency of evanescent FWM

$$\eta = \frac{P_{FWM}}{P_{pump}^2 P_{probe}} = 2 \times 10^{-12} mW^{-2}.$$

S3. Experimental Setup for Nonlinear Reflection Law's Demonstration

We demonstrate the nonlinear reflection law of degenerate four-wave mixing process through the reflective configuration shown in Fig. S6 ($\lambda/2$: half-wave plate, M: mirror, DM: dichroic mirror, Obj: objective lens, F: band-pass filter, EMCCD: electron-multiplying CCD).

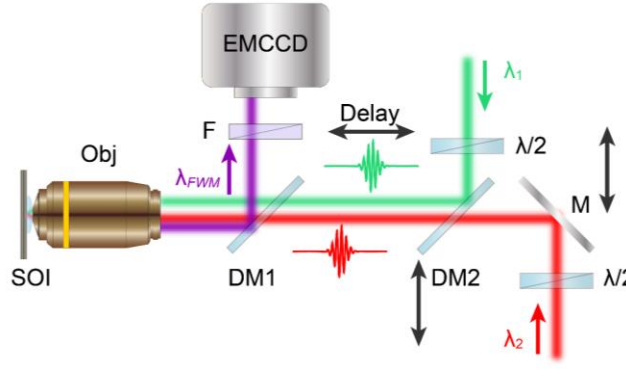


Fig. S6 Experimental setup of validating nonlinear reflection law

Incident angles of the pump/probe beams onto the substrate are controlled via relative distance of beam spot at the back aperture of the objective lens, by moving reflective and dielectric mirrors M, DM2 mounted on translational stages. A delay line is employed in the light path of pump beam to precisely control time delay between pump/probe pulses, with minimum time step of 1.67fs. The output signal is collected by the same objective and reflected by a dichroic mirror DM1 (Thorlabs), which transmits pump/probe beams and reflects signal beam. The FWM signal is detected by EMCCD (Andor iXon 879) placed after several narrow band-pass filter centered at 405nm. (From now on, λ_1 is called as pump beam, λ_2 as probe beam and λ_{FWM} as signal beam.)

S4. Pump, Probe and Signal beam's Angle Measurement

In our experiment, incident and output angles of pump, probe and signal beams are determined from reflected back-aperture images of the objective lens taken by EMCCD directly after objective lens (as the setup shown in Fig. S6. Part of the incident lights will also be reflected by DM1 because of imperfect transmission of DM1). The objective lens we used is well-corrected for aberration and chromatic dispersion, so we can simply consider a linear relationship between sine value of incident angles with spot distance from back-aperture center, described as $\sin(\theta) \propto r$. From this relationship, we can estimate sine values of angles directly:

$$\frac{r}{R} = \frac{n \sin(\theta)}{NA}$$

where R is the radius of back aperture, NA is numerical aperture of objective lens. For example, the distance between the spot position and back-aperture center can be estimated from the real experiment Fourier space image as Fig. S7 shows, hence corresponding angles can be determined by simple calculation.

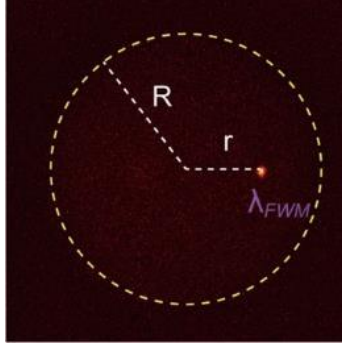


Fig. S7 One experimental Fourier space image of signal beam at λ_{FWM}

S5. Experimental Setup for FWM Signal Beam Imaging

Real-space images in our experiment at wavelength λ_{FWM} are taken by a home-built microscope [Fig. S8], modified based on setup shown in Fig. S6. Pump and probe beams pass through the dichroic mirror and interact together at the interface of nonlinear substrate. The excited FWM signal beam will be scattered by imaging targets deposited on substrate, carrying object information and being collected by the objective in the far-field. There is a relay lens pair placed after the tube lens of microscope to provide further magnification, whose focal position coincides with that of the tube lens.

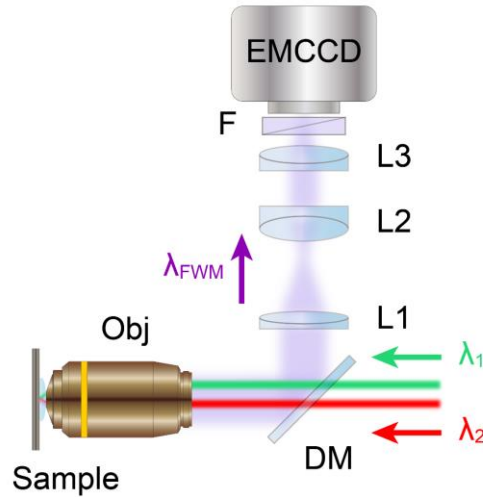


Fig. S8 Setup of home-built microscope used to take real space images

S6. Fourier Ptychography Reconstruction Routine and Phase-retrieval Ability

We follow Fourier ptychography technique to do image reconstruction. This technique requires multiple images taken under different, known illumination angles, represented by $I_m(k_{FWM,i}, 0)$ (m stands for

measurements, $k_{\text{FWM},i}$ denotes waves excited by FWM process with well-defined, large k vector in our method). The reconstruction routine is shown in Fig. S9.

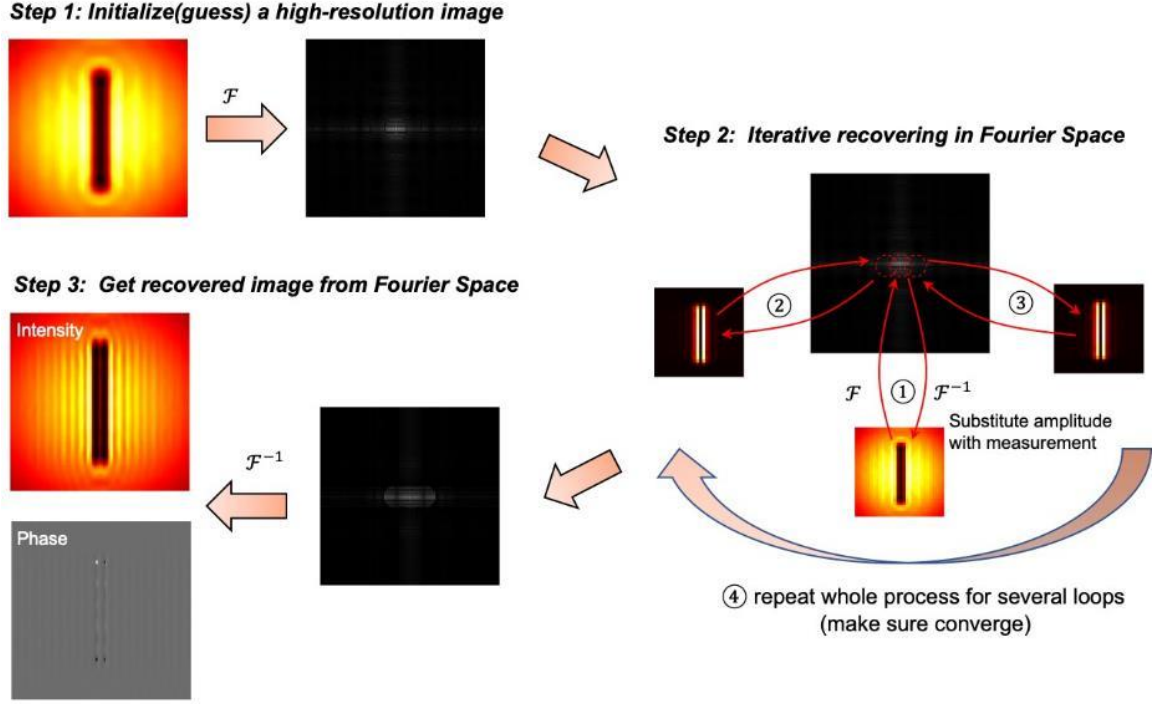


Fig. S9 Illustration of image reconstruction routine of Fourier ptychography

Firstly, we need to initialize a recovered high-resolution image I_h (h stands for high-resolution) either with random initialization or just interpolation of any experimental measurement. Then Fourier transform (FT) is applied to its complex field $\sqrt{I_h} e^{i\varphi_h}$ (phase φ_h can also be randomly initialized), generating a Fourier spectrum of the target corresponding to limited NA.

Step 2 is the most important part that we need to select out different parts of the spectrum centered at different illumination $k_{\text{FWM},i}$ with the radius equal to pass band of the objective $NA \times k_{\text{FWM,vac}}$ ($k_{\text{FWM,vac}}$ is wave vector of FWM in vacuum), successively. We need to do inverse FT over these parts successively, generating low-resolution target image $\sqrt{I_l} e^{i\varphi_l}$ (l: low-resolution) and then substitute real space image's amplitude measurement $\sqrt{I_m}$ with $\sqrt{I_l}$ under corresponding illumination angle. The whole recovering process of step 2 needs to be repeated over several times to make sure that the final reconstruction is convergent. This step will generate an enlarged area in Fourier spectrum with replenished high-frequency parts, which is the Fourier transform of $\sqrt{I_h} e^{i\varphi_h}$.

The final recovered intensity image as well as phase map can be obtained by doing inverse FT over the whole recovered spectrum. Finally, the recovered intensity image is square of the amplitude part and the phase map is simply phase part of the recovered complex image.

S7. Scanning Electron Microscope (SEM) Image of Slit Array

In Fig. 4 of our manuscript, we carry out our method imaging a slit array with slit width 110nm and period 400nm. Following is SEM image of the slit array target being measured in the manuscript.

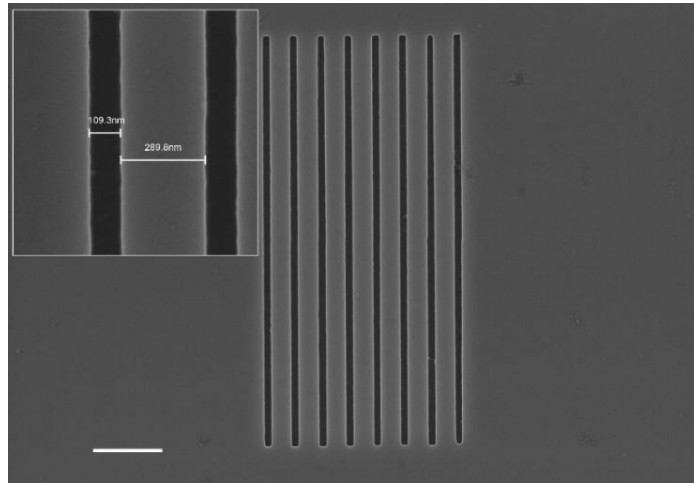


Fig. S10 SEM image of the slit array. Scale Bar: $1\mu m$

S8. Simulation of a 2D Target with Complex Shape and Size

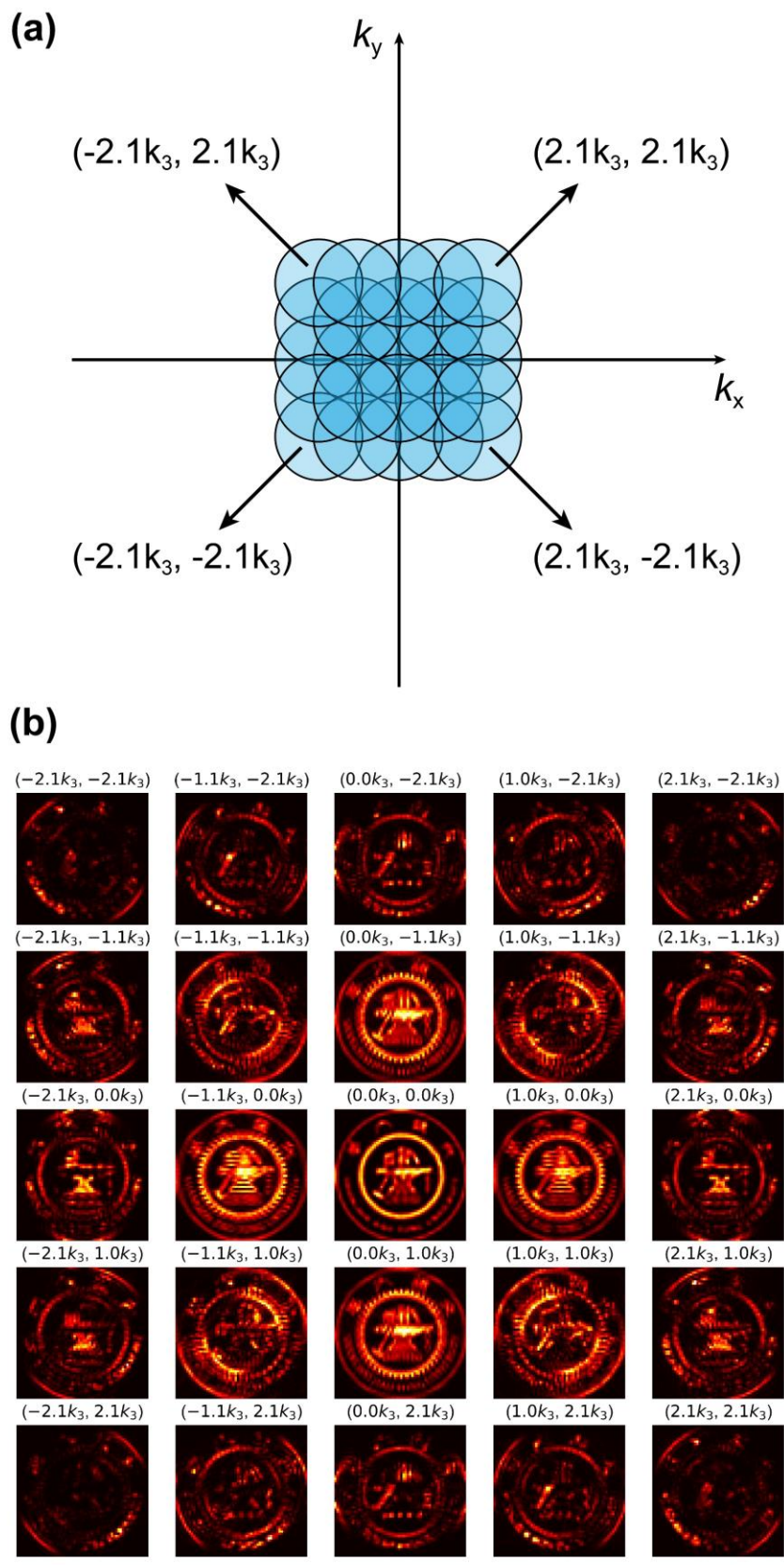


Fig. S11 Illustration of illumination scheme and far-field images under different illuminating wave vector
 (a) Illustration of illumination in Fourier space (b) Simulated corresponding far-field images

To give a more intuitive result, we simulated 2D scheme of our method by the emblem of our university, whose physical dimension is assumed as $6\mu m \times 6\mu m$. In the simulation, maximum wavenumber of evanescent wave is set as $3k_{FWM}$ ($3k_3$ in figure) and the illumination wavenumbers are equally spaced in the Fourier space to form a squared array of illumination [Fig. S11 (a)]. All of the simulated illuminations are evanescent since their wavenumbers are larger than the propagating one (k_3). Far-field images under different illumination pair (k_x, k_y) are presented in the Fig. S11 (b).

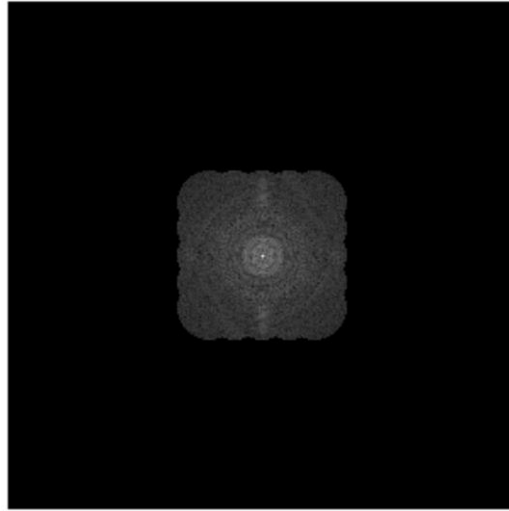


Fig. S12 Reconstructed Fourier spectrum of the emblem

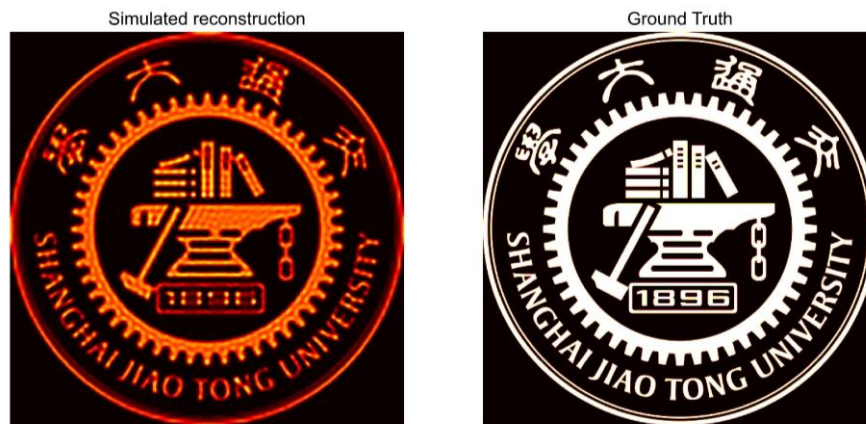


Fig. S13 Recovered SJTU emblem and ground truth

From a single image with large k illumination, we can hardly tell what the thing is because of the complexity of our simulated object as well as the coherent defects. But among which the information encoded are all high-frequency counterparts in the Fourier space, which is critical for sub-wavelength features far below diffraction limit. After iterative reconstruction by stacking together all these 25 images using FP technique, a complete Fourier spectrum of the objective can be recovered [Fig. S12], which is a convergent result of all those individual measurements. From the recovered image [Fig. S13], we can see significant improvements in the image resolution as compared to FWM normal illumination case $(0k_3, 0k_3)$, with most of the lost details get recovered in the final reconstruction, such as the gear and the letters, whose dimensions are far below the diffraction limit of the system.

S9. Comparison of Evanescent Wave Excitation on Bare Silicon and SOI

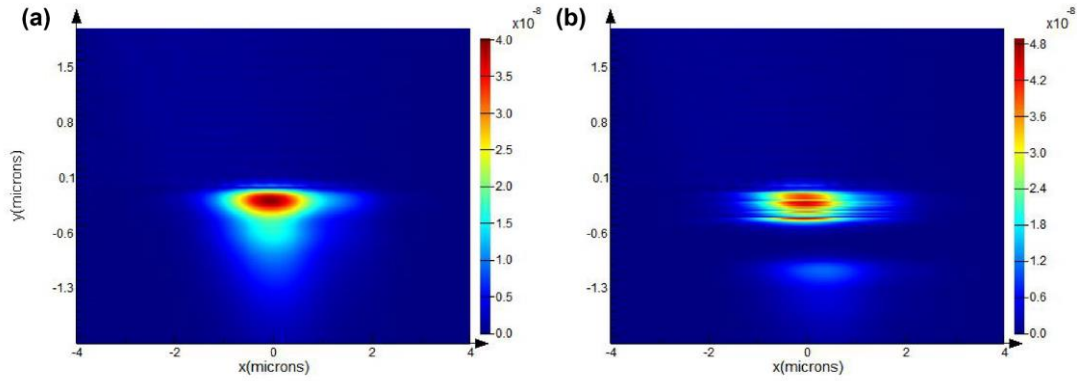


Fig. S14 FDTD simulation of evanescent wave generation by FWM (a) on bare Silicon (b) on SOI in our paper. The incident angles of pump/probe are set as the same to be 40°

We provide a simulated result of the two cases (FWM excitation on SOI substrate in our paper and bare silicon), where the incident angles of pump and probe beams are set equal but opposite to each other [Fig. S14]. We can see there is no significant difference between the two cases of FWM evanescent wave excitation except that the layered structure has some interference fringe pattern.

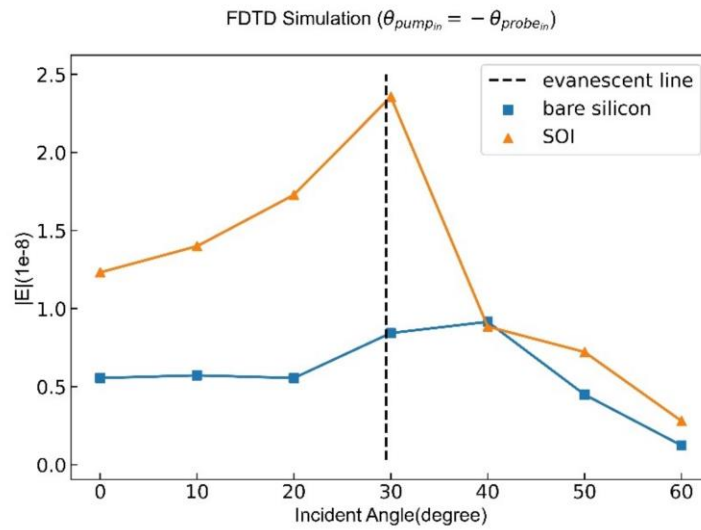


Fig. S15 Monitored magnitude at the center point of illumination

We also carry out a parameter sweep on incident angles and monitor the excited E magnitude at the center of light spot [Fig. S15]. As can be seen from Fig. S15, SOI does provide some enhancement with respect to bare silicon when the excited FWM is a propagating one, but there is also a significant drop of intensity when the excited FWM exceeds evanescent and the two cases are on the same level. We think this is because the transverse wave vector of evanescent wave makes the signal propagate along interface instead of into the substrate. Hence, we think that the enhancement of evanescent FWM excitation by SOI structure can be neglected here and this method can also work for a bare silicon substrate. Technically, our method can work for any material which possesses a relatively large $\chi^{(3)}$, such as semiconductors like Si, Ge, GaAs, etc.